Editors' Suggestion

Tunable magnetism in boron imidazolate based metal-organic frameworks

Jackson Davis,[1] Pilar Beccar-Varela,[2] Soumyodip Banerjee,[2] Maxime A. Siegler,[2] V. Sara Thoi,[2,3] and Natalia Drichko[1,*]

[1]*Department of Physics and Astronomy, Johns Hopkins University, Baltimore, Maryland 21218, USA*

[2]*Department of Chemistry, Johns Hopkins University, Baltimore, Maryland 21218, USA*

[3]*Department of Materials Science and Engineering, Johns Hopkins University, Baltimore, Maryland 21218, USA*

(Received 30 May 2024; revised 10 September 2024; accepted 6 November 2024; published 25 November 2024)

Magnetic metal-organic frameworks (MMOFs), where magnetic metal nodes are connected into a crystal structure by organic linkers, have a potential to host exotic magnetic states. We present a study of bulk magnetic properties of four metal-organic frameworks with the same boron imidazolate linkers, Cu-BIF, Co-BIF, Ni-BIF, and newly synthesized Zn-BIF, displaying a variety of lattice structures and nontrivial magnetic behaviors. While nonmagnetic Zn-BIF provides an offset of magnetic response, magnetic susceptibility measurements of the other three magnetic materials demonstrate the presence of weak magnetic interactions in these MOFs, which differ between materials by sign and size. Cu-BIF, where magnetic nodes are connected into octahedral cages, shows simple paramagnetic behavior. Triangular lattice Co-BIF shows antiferromagnetic interactions on the order of 1 K, and a spin-crossover-like effect in magnetic susceptibility due to thermal depopulation of excited crystal electric field levels. Magnetic properties of Ni-BIF suggest sizable ferromagnetic interactions. Using DC/AC susceptibility and variable-field DC magnetization, we detect cluster spin-glass behavior in Ni-BIF and discuss possible microscopic origins of this behavior. This work demonstrates the variety of magnetic properties possible with a single organic ligand and establishes the low energy scale of magnetic interactions through superexchange in boron imidazolate frameworks.

DOI: 10.1103/PhysRevB.110.184426

I. INTRODUCTION

Frustrated magnetism is one of the hot topics of current condensed matter research. While one of the ultimate goals is to synthesize and characterize spin liquid materials, where highly interacting spins are not ordered down to low temperatures [1,2], many exotic magnetic states and new materials are found as a part of this research. One underexplored source of new magnetic materials are magnetic metal-organic frameworks (MMOFs), in which metal nodes are connected into crystals by organic linkers [3]. Due to the versatility of organic chemistry and a relatively easy way to substitute metallic nodes without changing the structure or achieving different structures with the same magnetic nodes and linkers, these materials have the potential to be highly tunable magnets. There are a number of theoretical proposals on the realization of exotic magnetism in these materials [4–9], as well as a fair amount of MMOFs synthesized [3], but systematic studies of magnetic properties are rare.

In this manuscript, we present systematic magnetic studies of four boron imidazolate frameworks (BIFs), a unique subclass of MOFs that bear resemblances to zeolites and zeolitic imidazolate frameworks [10,11], pictured in Fig. 1. Controlling the synthetic conditions as well as selecting the identity of the metal ion precursor can lead to a variety of solid-state structures. In this study, we selected four BIFs that are supported by the same boron trisimidazolate linker, but with different metal ions. Co-BIF and Ni-BIF are isostructural and form layered structures of 2D triangular lattices of MN_6 octahedra [M = Co ($J = 1/2$), Ni ($S = 1$)] with D_{3d} symmetry, connected by boron imidazolate molecules. Cu-BIF forms a M_6L_8 (M = metal ion, L = ligand) cage structure, with six Cu^{2+} ions ($S = 1/2$) in an octahedral arrangement around a central pore. Finally, Zn-BIF forms a different cage structure (M_4L_4), with four Zn^{2+} ($S = 0$) ions in a tetrahedral arrangement around a central pore. These structures allow us to explore the effects of metal node substitution and MOF crystal structure on the magnetic properties of MMOFs.

II. METHODS

Powders of Co-BIF, Ni-BIF, and Cu-BIF were synthesized according to methods reported in Refs. [12,13,16].[1] The synthesis of Zn-BIF was adapted from a previous report of a similar Zn boron imidazolate cage [14]; experimental details for this newly reported material can be found in the supporting information [17]. Measurements of magnetic properties were performed using a Quantum Design Squid MPMS equipped with the ^{3}He cooling option, which allowed measurements down to 0.4 K for selected materials. DC magnetic susceptibility measurements of powders of Co-BIF, Ni-BIF, Cu-BIF, and Zn-BIF as a function of

*Contact author: drichko@jhu.edu

[1]We name the compounds by their transition metal for clarity; Co-BIF, Ni-BIF, and Cu-BIF were designated CoN_6-BIF, NiN_6-BIF, and BIF-29, respectively, in Refs. [12,13,16]

 ©2024 American Physical Society

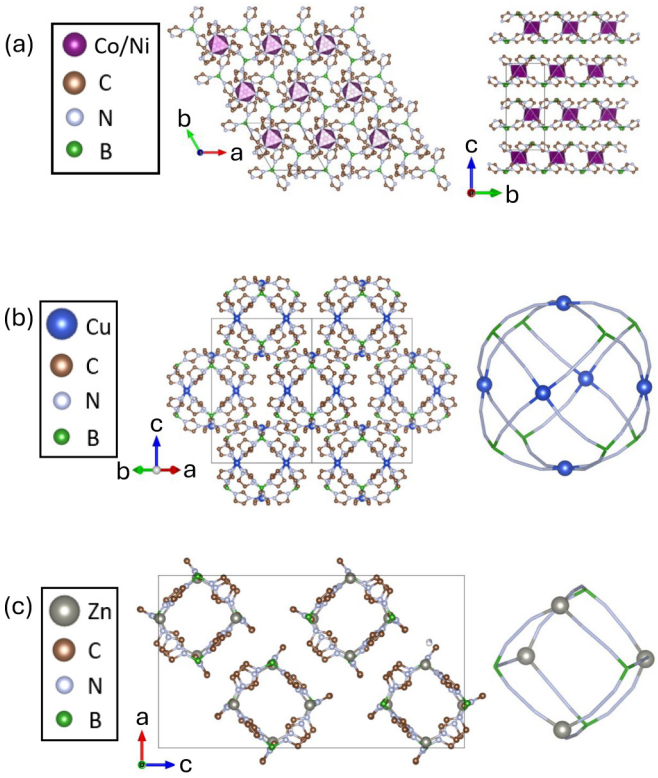

FIG. 1. Crystal structure of all four BIFs. (a) Structure of Co-BIF and Ni-BIF shown along crystallographic *c* axis, showing a triangular layer of Co/NiN_6 octahedra, and along crystallographic *a* axis, demonstrating stacking of layers [12]. (b) Packing of Cu-BIF cages and a single Cu-BIF cage schematic with ligands shown as rods [13]. (c) Packing of Zn-BIF cages and a single Zn-BIF cage schematic with ligands shown as rods [14]. Hydrogen and oxygen omitted from all structures to clearly show metal ions and ligands. All structures visualized in VESTA [15].

temperature χ(T) were performed in 2–300 K temperature range, with an extension down to 0.4 K for Co-BIF and Cu-BIF. All DC susceptibility measurements were performed with a $\mu_0 H = 0.1$ T applied magnetic field on warming. For the field-cooled measurements, the samples were cooled under the same 0.1 T magnetic field. Saturation fields measured for these compounds at minimal temperatures were on the order of 1 T, thus for this comparably small field we calculate magnetic susceptibility χ as $\chi = M/H$. Magnetization at 2 K and above was measured with magnetic field sweeps from −7 to 7 T. AC susceptibility measurements of zero-field cooled samples were performed with a 1 Oe AC magnetic field amplitude with no applied DC magnetic field. For all the measurements, a powder sample of MOF was wrapped in clear plastic wrap and inserted into a plastic straw fixed for the measurements in the MPMS. Magnetic response of the same wrap in a straw was measured prior to each set of the measurement parameters in order to subtract the background. The total mass of the samples used for the measurements was 5.57 mg Co-BIF, 1.67 mg and 9.05 mg Ni-BIF (9.05 mg data reported here), 3.77 mg Cu-BIF, 22.0 mg Zn-BIF. The data are normalized to mass/number of moles/number of magnetic ions depending on the measurement.

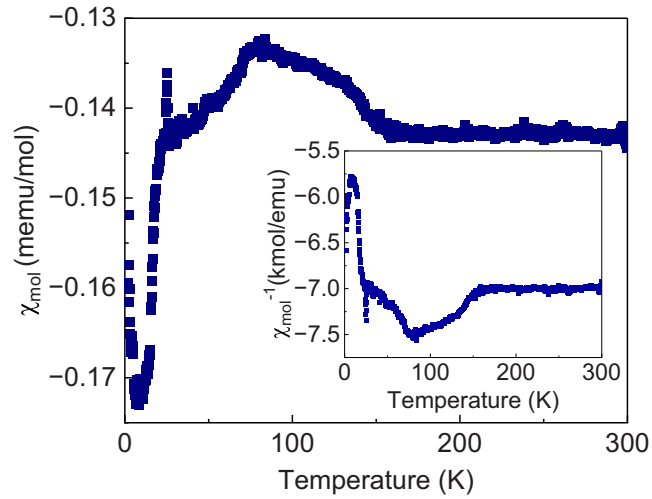

FIG. 2. Molar susceptibility vs temperature of diamagnetic Zn-BIF. Negative susceptibility that is several orders of magnitude smaller than other BIFs indicates diamagnetism. Deviations from constant susceptibility are attributed to artefacts in background subtraction. Inset: Inverse susceptibility of Zn-BIF vs. temperature.

III. RESULTS

A. Zn-BIF

With a fully occupied 3*d* electron shell, Zn^{2+} is expected to be nonmagnetic, resulting in a diamagnetic response of Zn-BIF. The structure of Zn-BIF, shown in Fig. 1(c), consists of cubic cages, where four Zn ions sit on opposite corners in a tetrahedral arrangement, and each Zn is connected to the others by 2 boron imidazolate linkers. As shown in Fig. 2, Zn-BIF displays a negative molar susceptibility that is about 4 orders of magnitude smaller than molar susceptibilities of the other MOFs studied in this work. The deviations from temperature-independent diamagnetic response are a result of the sample magnetization being on the same order of magnitude as the diamagnetic clear plastic wrap background, and thus incurring artefacts as a result of background subtraction.

This measurement suggests that the boron imidazolate linkers themselves are not inherently magnetic, and as a first approximation any magnetic response of other MOFs with the same linker most likely comes from the magnetic metal ions and their interactions mediated by the linkers.

B. Cu-BIF

Cu-BIF exhibits a cage structure which connects each of the six magnetic S=1/2 Cu^{2+} ions in an octahedral cage cluster as shown in Fig. 1(b). The Cu^{2+} ions are found in an anisotropic square pyramidal environment, with 4 N from the ligands forming the base of the pyramid and a weakly bound H_2O outside the cage forming the tip. Inverse magnetic susceptibility and magnetization of Cu-BIF are shown in Fig. 3. Inverse susceptibility is fit to a Curie-Weiss paramagnetic behavior with a weak constant susceptibility χ_0 [18]:

$$\chi^{-1} = \frac{T - \Theta_{CW}}{\chi_0 (T - \Theta_{CW}) + C}. \quad (1)$$

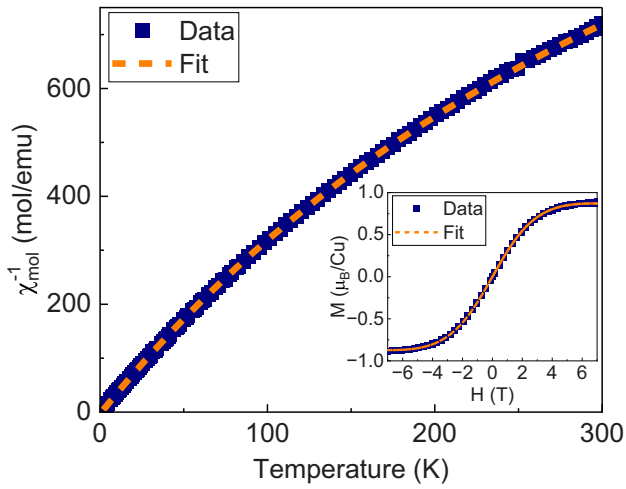

FIG. 3. Inverse susceptibility vs temperature of Cu-BIF, cooled in zero field, fit to a Curie-Weiss paramagnetic model. (Inset) Magnetization vs field of zero-field-cooled Cu-BIF at 2K, fit to Brillouin function for a $S = \frac{1}{2}$ paramagnet.

The fit suggests a ferromagnetic Curie-Weiss temperature Θ_{CW} of 0.9(1) K, a Curie-Weiss constant C of 0.2587(7) emu K mol^{-1}, and a positive constant offset χ_0 of 0.000526(3) emu/mol, leading to the slight downward curve in the inverse susceptibility. The constant $C = 0.26$ emu K mol^{-1} yields an effective moment of 1.44 μ_B, slightly lower than the expected 1.73 μ_B for Cu^{2+} ions with $S = \frac{1}{2}$ and $g = 2$. No signature of magnetic ordering is present down to $T = 0.4$ K (see Fig. 4(c) of Ref. [17]).

Magnetization at $T = 2$ K is also well fit by a Brillouin function for paramagnetic ions with $S = \frac{1}{2}$ plus a small temperature- and field-independent Van Vleck/diamagnetic

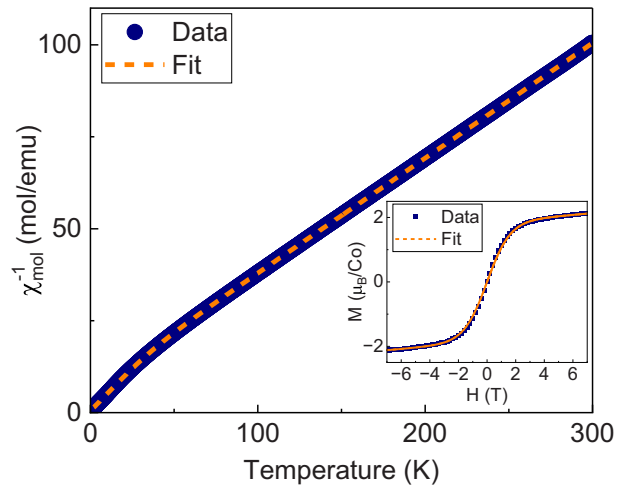

FIG. 4. Inverse susceptibility vs. temperature of Co-BIF, fit with a two-level thermal population model, with kink visible around 25 K. (Inset) Magnetization vs field of zero field-cooled Co-BIF at $T = 2$ K, fit to the Brillouin function for magnetization of a $J = \frac{1}{2}$ paramagnet.

susceptibility:

$$M = gJB_J\left(\frac{gJ\mu_B}{k_BT}H\right) + \chi_0 H. \tag{2}$$

The fit suggests $g = 1.966(1)$, giving a saturation moment of 0.983 μ_B/Cu, and $\chi_0 = -1.26(1) \times 10^{-2}\mu_B$/Cu/T.

C. Co-BIF

Co-BIF has a layered structure, where CoN_6 octahedra are connected by boron imidazolate ($HB(Im)_3$) molecules into a triangular lattice forming each layer. ($HB(Im)_3$) linkers connect CoN_6 octahedra on the top and bottom of each layer [see Fig. 1(a)].

Inverse susceptibility of Co-BIF and magnetization versus field are shown in Fig. 4. Inverse susceptibility deviates from Curie-Weiss behavior due to a kink around 25 K, which splits the inverse susceptibility into two linear regions with different slopes. Following Refs. [18,19], we fit $\chi^{-1}(T)$ with a model that takes into account the spin-orbit coupling of Co^{2+} and the orbital splitting in the octahedral nitrogen crystal field environment. The crystal electric field relieves the degeneracy of the $3d$ orbitals, resulting in a T_{2g} ground triplet which is further split by SOC into a low-spin $j = \frac{1}{2}$ ground state and a high-spin $j = \frac{3}{2}$ excited state. In a model for magnetic susceptibility, the thermal population of both levels is taken into account. The thermal population model replaces the Curie-Weiss constant $C = \mu^2_{\text{eff}}/8$ with a temperature-dependent factor reflecting the effective moment from thermal population of these states:

$$\chi^{-1} = 8(T - \Theta_{CW})\left(\frac{\mu^2_{\text{eff},0} + \mu^2_{\text{eff},1}e^{\frac{-E_1}{k_BT}}}{1 + e^{\frac{-E_1}{k_BT}}}\right)^{-1}, \tag{3}$$

where $\mu_{\text{eff},0}$ and $\mu_{\text{eff},1}$ are the effective moments of the ground and excited states, respectively, and E_1 is the energy gap between these states. The fit suggests $\Theta_{CW} = -1.18(3)K$, effective moments $\mu_{\text{eff},0} = 4.052(3)\mu_B$ and $\mu_{\text{eff},1} = 5.734(2)\mu_B$, and a gap $E_1 = 96.9(3)$ K.

Magnetization at T = 2 K is fit to a paramagnetic Brillouin function for $J = \frac{1}{2}$ with a linear contribution from constant susceptibility. The fit suggests $g = 3.78104(5)$, similar to other Co triangular lattice materials [19]. With $j_{\text{eff}} = \frac{1}{2}$, this results in a saturation moment of 1.89 μ_B/Co. The linear contribution is $\chi_0 = 2.98(3) \times 10^{-2}\mu_B$/Co/T, similar in magnitude to Cu-BIF, but positive, indicating a larger Van Vleck paramagnetic contribution. Following Ref. [19], we additionally fit the data to a delayed Brillouin function, reflecting an exchange field experienced by each Co moment due to magnetization of the sample and exchange interactions with neighboring moments. However, the fit did not significantly improve upon inclusion of this exchange field, reflecting weak exchange interactions between Co magnetic moments.

D. Ni-BIF

Ni-BIF, which is isostructural to Co-BIF [see Fig. 1(a)] but contains S = 1 Ni^{2+} ions, displays different magnetic behavior. The inverse susceptibility fit above 100 K suggests larger interactions which are ferromagnetic, with $\Theta_{CW} = 16.5(1)$ K.

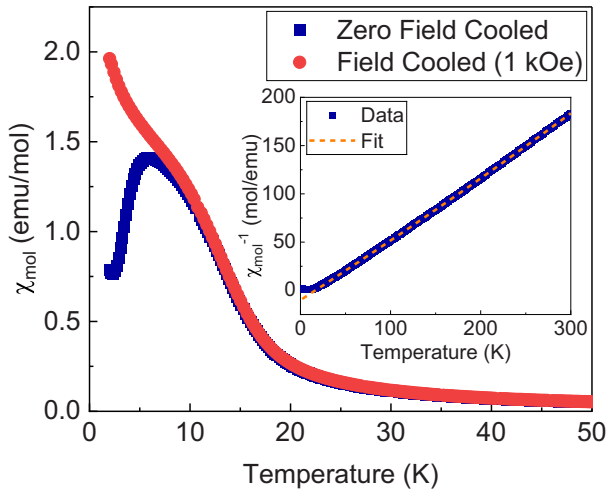

FIG. 5. Magnetic susceptibility vs. temperature of Ni-BIF, cooled in both zero field and 1000 Oe applied field. (Inset) Inverse magnetic susceptibility fit above 100 K to Curie-Weiss paramagnetic susceptibility.

The fit also yields $C = 1.644(2)$, equating to an effective moment of 3.63 μ_B, larger than the expected 2.83 μ_B for $S = 1$ and $g = 2$, and $\chi_0 = -0.000349(6)$ emu/mol. A divergence between zero-field cooled (ZFC) and 0.1 T field-cooled (FC) susceptibility is observed just below 10 K, shown in Fig. 5, with the ZFC susceptibility reaching a maximum at 6 K.

Since this result suggests magnetic interactions at least one order of magnitude higher than that in the isostructural Co-BIF, we first performed tests which confirmed that this result is an intrinsic behavior of Ni-BIF: (i) to test for possible contamination, magnetic behavior of the chemical precursor, $Ni(NO_3)_2 \cdot 6H_2O$, was measured and is shown to be essentially different from the magnetic behavior of Ni-BIF (see Fig. 6(d) of Ref. [17]). (ii) The chemical composition of the powders was confirmed by Raman spectroscopy [20]. (iii) Reproducibility was confirmed for 2 different samples from different synthesized batches. Magnetic susceptibility of the two batches is presented in Fig. 6(c) of Ref. [17].

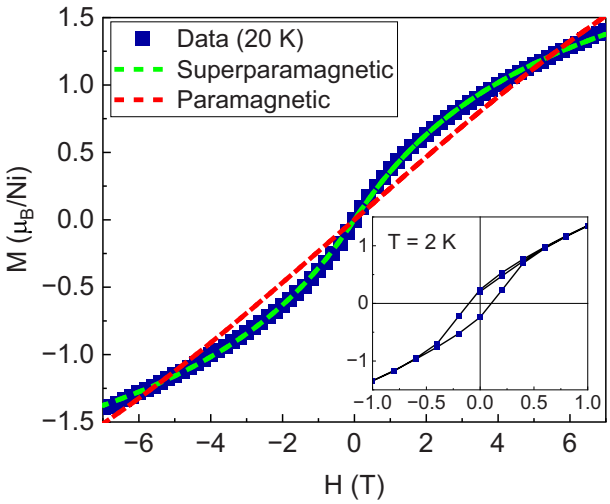

FIG. 6. Magnetization vs field of Ni-BIF at 20 K, fit to a magnetization of a distribution of superparamagnetic nanoparticles, as well as best fit to a Brillouin magnetization function for a $J = 1$ paramagnet. Inset: Magnetization vs field at $T = 2$ K, showing hysteresis.

Isothermal magnetization also demonstrates a deviation from a paramagnetic behavior in contrast to the other MOFs studied in this work, see Fig. 6. For magnetization measured at 20 K, above the region of susceptibility divergence, the Brillouin function for $S = 1$ paramagnetic moments does not fit the measured curve. Magnetization measured at $T = 2$ K, below the region of divergence between ZFC and FC susceptibility, recovers paramagnetic behavior on the larger magnetic field scales, but displays a small hysteresis loop with a coercive field of ~0.1 T (see inset in Fig. 6).

The crossover behavior and a difference between FC and ZFC states for magnetic susceptibility, together with magnetization deviating from a Brillouin function at temperatures above the crossover, and a hysteresis present in the low-temperature frozen state are characteristic of cluster spin glasses [21,22]. Here the frozen moments are related to the ordered clusters of spins rather than single spins. Similar to superparamagnetic heterogeneous nanoparticles, magnetization above the blocking temperature is determined by the presence of a distribution of magnetic moments of different magnitudes [23,24].

We thus fit the magnetization at $T = 20$ K with a method inspired by Ref. [23]. This model assumes a modified log-normal distribution of nanoparticle magnetic moments with median moment μ_0 and standard deviation σ:

$$f(\mu) = \frac{N}{\sqrt{2\pi}\sigma\mu} \exp\left(-\frac{\ln \frac{\mu}{\mu_0}^2}{2\sigma^2}\right). \tag{4}$$

For superparamagnetic nanoparticles, a magnetization would result in an integration over a continuous range of moments μ, each described by a Langevin function. However, we obtain the best fit using a discrete sum of Brillouin functions of magnetic moments of small clusters of spins:

$$M = \sum_{J=1}^{100} gJB_J\left(\frac{gJ\mu_B H}{k_B T}\right) P(J), \tag{5}$$

where B_J is the Brillouin magnetization function for total angular momentum quantum number J and the weight $P(J)$ is given by a discretization of the above log-normal distribution, now using integer J values instead of continuous μ:

$$P(J) = \int_{J-0.5}^{J+0.5} f(J, J_0, \sigma) dJ. \tag{6}$$

The parameters of the best fit are $g = 2.2(8)$, standard deviation $\sigma = 1.30(2)$ of the quantity $\ln(\frac{\mu}{\mu_0})$, and median moment $J_0 = 0.5(2)$ of the continuous log-normal distribution, which equates to a median moment of $J_0 = 1$ when converted to the discrete distribution shown in Fig. 7. The small median moment is an indication that clusters are on the scale of single unit cells, and thus the possibility of superparamagnetic nanoparticles can be rejected in favor of a cluster spin-glass state. The distribution of moments that reproduces the observed magnetization is restricted by the modified log-

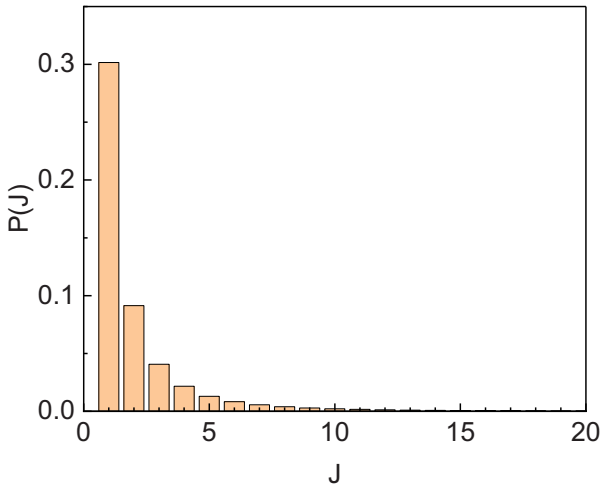

FIG. 7. Discrete log-normal distribution of moments in Ni-BIF obtained from fit to Eq. (5) of $T = 20$ K magnetization data.

normal distribution used for nanoparticles for fitting purposes; nevertheless, the fit proves that a small percentage of higher moments among a majority of $J = 1$ single paramagnetic moments is necessary to describe the data.

At $T = 2$ K, below the crossover, the magnetization vs. field data are well fit by a single paramagnetic response, with the exception of the hysteresis loop. The fit to a Brillouin function for a $J = 1$ paramagnet suggests $g_J = 2.400(4)$, with a field-independent linear contribution of $\chi_0 = 8.4(1) \times 10^{-2}\,\mu_B$/Ni/T. The adherence of the data to a single Brillouin function suggests that a single species of moment, the single-spin $J = 1$ moment, dominates the magnetization response at this temperature.

To further understand the temperature-dependent spin relaxation dynamics of Ni-BIF we performed ZFC AC susceptibility measurements on the same sample. In-phase susceptibility χ' is shown in Fig. 8(a) for five different frequencies with zero applied DC field. The χ' data have been normalized to the high-temperature susceptibility at 999 Hz in order to clearly show the evolution of the freezing temperature T_f. Raw data are presented in Fig. 7(b) of Ref. [17]. χ' displays a broad, complex peak shape consistent with a broad crossover in DC magnetic susceptibility (Fig. 5). The peak in χ' shifts to higher temperatures as frequency is increased. The out-of-phase component χ'', shown in Fig. 7(c) of Ref. [17], highlights the complex peak shape. T_f is approximated from the maximal point on the high-temperature side of the broad peak, as shown in Fig. 8(a). T_f changes from 11.7 to 12.5 K between 1 and 999 Hz; thus the Mydosh parameter, $\Delta T_f/(T_f \log_{10}(\Delta\nu))$, or the fractional change in T_f per decade of frequency, is found to be 0.02. This parameter can be used to distinguish between spin-glass and superparamagnetic states, as in conventional spin-glasses it is found to be $\lesssim$0.01 while in superparamagnets it is $\gtrsim$0.1 [22,25]. An intermediate value such as that observed for Ni-BIF is attributed to cluster spin-glass behavior [21,25].

An estimation of characteristic relaxation times allows to distinguish between spin glass and cluster spin glass [21,25]. Relaxation time can be estimated using the Vogel-

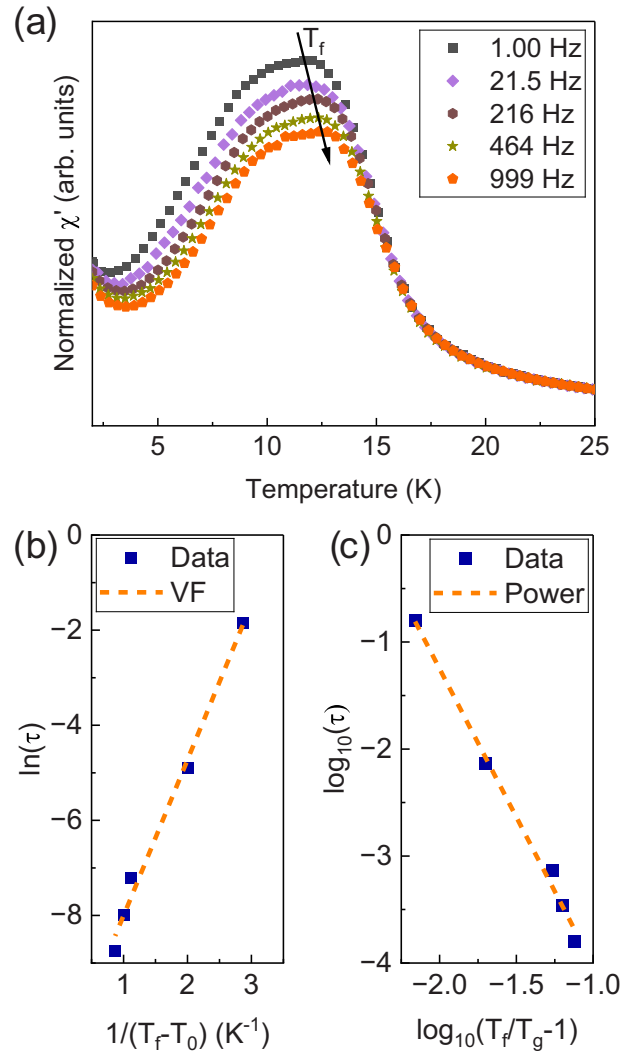

FIG. 8. (a) In-phase component of AC susceptibility of Ni-BIF. χ' data have been normalized to high-temperature χ' at 999 Hz; raw data and scaling factors are presented in Ref. [17]. (b) Vogel-Fulcher fit to T_f obtained from χ'. (c) Power law fit to T_f obtained from χ'.

Fulcher model [see Fig. 8(b)] which adapts the noninteracting Néel-Arrhenius law with a phenomenological parameter T_0 accounting for intercluster interactions [26]:

$$\tau = \tau_0 \exp(E_a/k_B(T_f - T_0)), \tag{7}$$

where $\tau = 1/2\pi\nu$. The fit suggests a characteristic relaxation time $\ln(\tau_0) = -11(1)$ [$\tau_0 \sim 2.5(2.0) \times 10^{-5}$ s], an energy barrier $E_a/k_B = 3(2)$ K, and a VF temperature $T_0 = 11.2(2)$ K. Relaxation times of 10^{-7}–10^{-10} s are associated with cluster spin glass, while shorter times of 10^{-12}–10^{-14} s are associated with conventional spin-glass systems [25]. The timescale derived for Ni-BIF is slower than either of these, but more consistent with cluster spin-glass than spin-glass behavior.

An alternative way to estimate relaxation times is to use a power law describing critical slowing down of the relaxation time near the crossover [26]:

$$\tau = \tau^*(T_f/T_g - 1)^{-z\nu'}, \tag{8}$$

TABLE I. Oxidation states, total angular momentum quantum numbers J and Curie-Weiss Temperatures Θ_{CW} of BIFs.

BIF	structure	Ion	J	Θ_{CW} (K)
Zn-BIF	cage	Zn^{+2}	0	–
Cu-BIF	cage	Cu^{+2}	1/2	0.9
Co-BIF	triangular	Co^{+2}	1/2	−1.18
Ni-BIF	triangular	Ni^{+2}	1	16.5

where τ^* is a characteristic relaxation time similar to τ_0, T_g is the spin-glass temperature at zero frequency, and the power zv', which is treated as a single value for the fit, is the dynamical critical exponent for the relaxation time near the crossover. The fit in Fig. 8(c) suggests $\log_{10}(\tau^*) = -6.8(7)$ [$\tau^* \sim 4.1(3.8) \times 10^{-7}$ s], $T_g = 11.62(4)$ K, and $zv' = 2.8(6)$ K. The suggested ranges of the characteristic relaxation time and the dynamical critical exponent overlap with the ranges of 10^{-7}–10^{-10} s and 3–10 typically observed in cluster spin-glass systems [21].

IV. DISCUSSION

The different magnetic properties of the four BIFs, summarized in Table I, suggest the pathways of tuning magnetism of MMOFs by substitution of magnetic metal nodes and synthesis of different crystal structures with the same linker. Diamagnetism in Zn-BIF is expected, and suggests a "base line" to estimate magnetic behavior of magnetic materials of this group.

Cu-BIF demonstrates robust paramagnetic behavior. In its structure, each of the six Cu atoms are connected to each other by two boron imadozolate linkers, forming an octahedral cage. While we expect such pathways to provide small magnetic exchange, in agreement with $\Theta_c = 0.9\ K$, an absence of magnetic exchange pathways between the cages of six Cu atoms provides only a potential possibility for dipole-dipole interactions. Values of g, the effective moment, and the saturation moment in Cu-BIF are all slightly suppressed from the expected values for single noninteracting electron spins.

In the 2D structure of Co-BIF and Ni-BIF, each magnetic node is connected to the other ones by two pathways, "above" and "below" the layer of octahedra (see Fig. 1). We expect such structure to provide larger magnetic interactions, while a highly frustrated triangular lattice would prevent magnetic ordering at temperatures close to Curie-Weiss temperature [1]. An unexpected result is the ferromagnetic interactions and cluster spin glass behavior in Ni-BIF.

Co-BIF is an antiferromagnet with rather low values of magnetic exchange, as evidenced from $\Theta_{CW} = -1.18$ K. It is interesting to compare this material to an inorganic triangular lattice of Co octahedra, $Na_2BaCo(PO_4)_2$ [19,27,28]. The Curie-Weiss temperature of $\Theta_{CW} = -1.18$ K of Co-BIF is roughly half of that for $Na_2BaCo(PO_4)_2$, $\Theta_{CW} = -2.5$ K [27], indicating that interactions between spins are reduced by superexchange through boron imidazolate, but still present. Indeed, while for $Na_2BaCo(PO_4)_2$ antiferromagnetic exchange J is found to be 1.37 K from the Brillouin function for $J = \frac{1}{2}$ with exchange field delay, antiferromagnetic exchange in Co-BIF is too small to change purely paramagnetic behavior at 2 K.

Similar to $Na_2BaCo(PO_4)_2$, temperature dependence of magnetic susceptibility of Co-BIF is determined by thermal population of low $j = \frac{1}{2}$ and high $j = \frac{3}{2}$ spin states split by spin-orbit coupling and crystal field due to trigonal distortion of Co-centered octahedra [19,29]. The gap between $j = \frac{1}{2}$ and $\frac{3}{2}$ in Co-BIF is 96.9 K, which is roughly 4 times smaller that the gap found in $Na_2BaCo(PO_4)_2$. This suggests a very small trigonal distortion of the Co octahedra [29], intuitively expected for a large cell and weaker interactions in a molecular crystal. From magnetization measurements done on powders, $g = 3.78$ is close to 4.38 for $Na_2BaCo(PO_4)_2$. Using $g = 3.78$ obtained from magnetization, we calculated expected effective magnetic moments 3.29 and 7.36 μ_B for the two levels in the population model. While the moment for $j = \frac{1}{2}$ is close to the observed 4.05 μ_B, the value for $j = \frac{3}{2}$ is deviating from the observed 5.73 μ_B.

Unexpectedly, triangular lattice 2D Ni-BIF, which is isostructural to Co-BIF [12], and shows similar vibrational spectrum [20], demonstrates very different magnetic behavior. Temperature dependence of magnetic susceptibility shows a broad peak of a crossover at around $T = 8$ K, with the divergence in susceptibility between ZFC and FC at $T = 10$ K, typical for a spin glass. Curie-Weiss temperature $\Theta_{CW} = 16.5$ K suggests ferromagnetic interactions of much higher magnitude than interactions in the other BIF MOFs. Magnetization at $T = 20$ K shows superparamagnetic behavior resembling that observed in cluster spin-glass systems or superparamagnetic nanoparticles. The small median magnetic moment parameter $J_0 = 1$, that results from the fit to a distribution of superparamagnetic nanoparticles, points to magnetic clusters on the scale of single unit cells rather than superparamagnetic nanoparticles with diameters of several nm. AC susceptibility measurements provide the estimation of the relaxation times using both Vogel-Fulcher and power law scaling models. Relaxation times of 10^{-5}–10^{-8} s are in the range expected for cluster spin glass. Finally, cluster spin glass description of magnetic behavior of Ni-BIF is confirmed by the Mydosh parameter.

A combination of magnetic frustration, competing antiferro- and ferromagnetic interactions, and disorder is a typical origin of cluster spin glass behavior [22]. While further research is necessary to exactly identify the microscopic origin of relatively large ferromagnetic interactions in triangular lattice Ni-BIF, we can speculate on it. A conversion of weaker antiferromagnetic exchange interactions into one order of magnitude stronger ferromagnetic interactions has been achieved in a magnetic MOF when adding an electron on a linker molecule by doping [30]. The extra electron in the radical linker interacting antiferromagnetically with each of the nodes provides the FM exchange between the metal nodes. Along these lines, we can suggest a concentration of disordered radical spins on some of the linkers. Since each linker binds to three metal nodes in this structure, a single radical could create a cluster of ferromagnetically ordered spins that sits in a lattice of much weaker AFM interactions.

A Raman scattering study of a MOF with a ligand containing an aromatic ring showed that the molecular vibrational

modes of the bonds associated with this ring changed significantly upon addition of a radical electron spin [31]. In our previous Raman scattering study of BIFs, we observed no significant change in these high-energy vibrational modes of the imidazole ring [20], indicating that these radicals may be localized to the boron in the linker rather than the imidazolate rings.

V. CONCLUSION

In this work, we demonstrate, using an example of metal-organic frameworks with imidazole-based linkers, robust magnetism of MOFs with magnetic nodes and tunability of magnetic properties (Table I). No magnetic response was observed for Zn-BIF with nonmagnetic node, while a cage structure of Cu-BIF shows paramagnetism with parameters expected for Cu^{2+} $S = 1/2$ and very weak FM interactions. The triangular lattice structures of Co-BIF and Ni-BIF demonstrate magnetic properties of interest. Co-BIF shows weak AF interactions and single-ion magnetism similar to inorganic materials. Ni-BIF shows sizable FM interactions and cluster spin-glass behavior which we attribute to disordered radical spins on the ligand. These results highlight the possibility of leveraging the inherent chemical tunability of MOFs to realize a variety of magnetic systems, especially when using different ligands that mediate stronger superexchange interactions.

ACKNOWLEDGMENTS

The authors are grateful to C. Broholm and K. Thirunavukkuarasu for discussions. Acknowledgment is made to the donors of the American Chemical Society Petroleum Research Fund Grant No. 61764-ND10 for partial support of this research. J.D. and N.D. acknowledge the support of NSF Award No. DMR-2004074. P.B.-V., S.B., and V.S.T. acknowledge support by the U.S. Department of Energy (DOE), Office of Science, Office of Basic Energy Sciences, Catalysis Science program, under Award DE-SC0021955. P.B.-V. also thanks the Dean's ASPIRE grant from the Office of Undergraduate Research, Scholarly and Creative Activity at Johns Hopkins University.

[1] L. Balents, Spin liquids in frustrated magnets, Nature (London) **464**, 199 (2010).
[2] C. Broholm *et al.*, Quantum spin liquids, Science **367**, 6475 (2020).
[3] A. E. Thorarinsdottir, and T. D. Harris, Metal-organic framework magnets, Chem. Rev. **120**, 8716 (2020).
[4] A. C. Jacko, C. Janani, K. Koepernik, and B. J. Powell, Emergence of quasi-one-dimensional physics in a nearly-isotropic three-dimensional molecular crystal: *Ab initio* modeling of $Mo_3S_7(dmit)_3$, Phys. Rev. B **91**, 125140 (2015).
[5] M. G. Yamada, H. Fujita, and M. Oshikawa, Designing Kitaev spin liquids in metal-organic frameworks, Phys. Rev. Lett. **119**, 057202 (2017).
[6] M. G. Yamada, V. Dwivedi, and M. Hermanns, Crystalline kitaev spin liquids, Phys. Rev. B **96**, 155107 (2017).
[7] W. Jiang, X. Ni, and F. Liu, Exotic topological bands and quantum states in metal–organic and covalent–organic frameworks, Acc. Chem. Res. **54**, 416 (2021).
[8] X. Zhang, Y. Zhou, B. Cui, M. Zhao, and F. Liu, Theoretical discovery of a superconducting two-dimensional metal–organic framework, Nano Lett. **17**, 6166 (2017).
[9] T. Kambe *et al.*, Redox control and high conductivity of nickel bis (dithiolene) complex π-nanosheet: A potential organic two-dimensional topological insulator, J. Am. Chem. Soc. **136**, 14357 (2014).
[10] H.-X. Zhang, M. Liu, T. Wen, and J. Zhang, Synthetic design of functional boron imidazolate frameworks, Coord. Chem. Rev. **307**, 255 (2016).
[11] V. I. Isaeva, K. E. Papathanasiou, and L. M. Kustov, Zeolite-like boron imidazolate frameworks (BIFs): Synthesis and application, Crystals **10**, 617 (2020).
[12] S. Banerjee, X. Han, M. A. Siegler, E. M. Miller, N. M. Bedford, B. C. Bukowski, and V. S. Thoi, Flexible 2D Boron imidazolate framework for polysulfide adsorption in lithium-sulfur batteries, Chem. Mater. **34**, 10451 (2022).
[13] S. Banerjee, J. M. Gorham, P. Beccar-Varela, H. G. Hackbarth, M. A. Siegler, N. Drichko, J. T. Wright, N. M. Bedford, and V. S. Thoi, Atomically dispersed CuN_x sites from thermal activation of boron imidazolate cages for electrocatalytic methane generation, ACS Appl. Energy Mater. **6**, 9044 (2022).
[14] T. Wen, and J. Zhang, Rational design of metal boron imidazolate cages to frameworks, Inorg. Chim. Acta **460**, 89 (2017).
[15] K. Momma, and F. Izumi, *VESTA 3* for three-dimensional visualization of crystal, volumetric and morphology data, J. Appl. Crystallogr. **44**, 1272 (2011).
[16] C. S. Gerke *et al.*, Electrochemical C-N bond formation within boron imidazolate cages featuring single copper sites, J. Am. Chem. Soc. **145**, 26144 (2023).
[17] See Supplemental Material at http://link.aps.org/supplemental/10.1103/PhysRevB.110.184426 for additional information on crystal structure, background subtraction, and reproducibility.
[18] S. Mugiraneza, and A. M. Hallas, Tutorial: A beginner's guide to interpreting magnetic susceptibility data with the Curie-Weiss law, Commun. Phys. **5**, 95 (2022).
[19] C. Wellm *et al.*, Frustration enhanced by Kitaev exchange in a $j_{\text{eff}} = 1/2$ triangular antiferromagnet, Phys. Rev. B **104**, L100420 (2021).
[20] J. Davis, S. Banerjee, P. Beccar-Varela, V. S. Thoi, and N. Drichko, Raman scattering spectra of boron imidazolate frameworks containing different magnetic ions, J. Chem. Phys. **158**, 214707 (2023).
[21] S. Banerjee, D. P. Panda, P. Yanda, and A. Sundaresan, Canonical spin glass and cluster glass behavior in the polymorphs of $LiFeSnO_4$, Phys. Rev. Mater. **7**, 034405 (2023).
[22] J. A. Mydosh, Spin glasses: redux: An updated experimental/materials survey, Rep. Prog. Phys. **78**, 052501 (2015).
[23] E. Ramírez-Meneses *et al.*, Superparamagnetic nickel nanoparticles obtained by an organometallic approach, J. Nanopart. Res. **13**, 365 (2011).

[24] E. F. Ferrari, F. C. S. da Silva, and M. Knobel, Influence of the distribution of magnetic moments on the magnetization and magnetoresistance in granular alloys, Phys. Rev. B **56**, 6086 (1997).

[25] P. Bag, P. R. Baral, and R. Nath, Cluster spin-glass behavior and memory effect in $Cr_{0.5}Fe_{0.5}Ga$, Phys. Rev. B **98**, 144436 (2018).

[26] J. Souletie, and J. L. Tholence, Critical slowing down in spin glasses and other glasses: Fulcher versus power law, Phys. Rev. B **32**, 516 (1985).

[27] N. Li *et al.*, Possible itinerant excitations and quantum spin state transitions in the effective spin-1/2 triangular-lattice antiferromagnet $Na_2BaCo(PO_4)_2$, Nat. Commun. **11**, 4216 (2020).

[28] R. Zhong, S. Guo, G. Xu, Z. Xu, and R. J. Cava, Strong quantum fluctuations in a quantum spin liquid candidate with a Co-based triangular lattice, Proc. Natl. Acad. Sci. USA **116**, 14505 (2019).

[29] B. S. Mou *et al.*, Comparative raman scattering study of crystal field excitations in co-based quantum magnets, Phys. Rev. Mater. **8**, 084408 (2024).

[30] P. Perlepe *et al.*, Metal-organic magnets with large coercivity and ordering temperatures up to 242 °C, Science **370**, 587 (2020).

[31] L. Liu, J. A. DeGayner, L. Sun, D. Z. Zee, and T. D. Harris, Reversible redox switching of magnetic order and electrical conductivity in a 2D manganese benzoquinoid framework, Chem. Sci. **10**, 4652 (2019).